

Influence of interface exchange coupling in perpendicular anisotropy [Pt/Co]₅₀/TbFe bilayersS. Mangin,^{1,2} T. Hauet,^{1,2} P. Fischer,³ D. H. Kim,⁴ J. B. Kortright,⁵ K. Chesnel,⁶ E. Arenholz,⁶ and Eric E. Fullerton⁷¹*San Jose Research Center, Hitachi Global Storage Technology, San Jose, California 95120, USA*²*Laboratoire de Physique des Matériaux, Nancy Université, Nancy, France F-54506*³*Center for X-ray Optics, Lawrence Berkeley National Laboratory, Berkeley, California 94720, USA*⁴*Department of Physics, Chungbuk National University, Cheongju 361-763, Republic of Korea*⁵*Materials Sciences Division, Lawrence Berkeley National Laboratory, Berkeley, California 94720, USA*⁶*Advanced Light Source, Lawrence Berkeley National Laboratory, Berkeley, California 94720, USA*⁷*Center for Magnetic Recording Research, University of California, San Diego, La Jolla, California 92093-0401, USA*

(Received 10 October 2007; revised manuscript received 7 April 2008; published 21 July 2008)

We present the magnetization evolution of perpendicular anisotropy TbFe and [Co/Pt]₅₀ thin films either in direct contact resulting in antiferromagnetic interfacial coupling or separated by a thick decoupling Pt layer. Magnetometry and x-ray magnetic circular dichroism spectroscopy determine the spatially averaged magnetic properties. Resonant magnetic x-ray small-angle scattering and magnetic soft x-ray transmission microscopy probed the domain configurations and correlations in the reversal processes. While the Co/Pt multilayer reverses by domain propagation, the TbFe magnetization reversal was dominated either by coherent magnetization reversal processes or by lateral domain formation depending on the interface exchange coupling. In the presence of lateral domains, dipolar field induced domain replication phenomena were observed.

DOI: [10.1103/PhysRevB.78.024424](https://doi.org/10.1103/PhysRevB.78.024424)

PACS number(s): 75.25.+z, 75.60.Ch, 75.60.Jk

I. INTRODUCTION

In the past decade considerable experimental and theoretical work has been devoted to study the role of interface exchange coupling on magnetization reversal processes in multilayer magnetic thin films. It has been extensively studied both for its fundamental understanding¹⁻³ and for potential applications.^{4,5} Lately, interest in antiferromagnetically coupled multilayers has grown for materials exhibiting strong perpendicular anisotropy.⁶ The physics of such systems is surprisingly complex.⁷ New magnetic states can be induced due to the competition between the various intrinsic (anisotropy and exchange coupling) and extrinsic (Zeeman, strain, and thermal) interactions. For perpendicular anisotropy systems with antiferromagnetic interlayer coupling, the exchange coupling tends to force an antiparallel alignment of the layer magnetizations whereas the dipolar and Zeeman interaction favor a parallel arrangement. Also in perpendicular films, the Zeeman and exchange interactions favor uniform lateral magnetization while dipolar interactions are inclined to create lateral domains.⁸ The competition between short-range exchange interactions and long-range dipolar interactions lead to various stable magnetic configurations and reversal mechanisms.^{6,9} Given the rich and diverse physics of these structures, only limited studies have been performed on such systems.^{7,10-15} A difficulty to understand these systems comes from the fact that even three-dimensional (3D) micromagnetic calculations do not reproduce all the features of the experimental data since such calculations cannot easily describe both exchange-dominated interfacial domain walls at the atomic scale and lateral domain formation at the micrometer scale driven by long-range dipolar fields.

In this paper, we describe the evolutions of the magnetic configurations in a bilayer structure of perpendicular anisotropy [Pt/Co]₅₀ multilayer and a TbFe ferrimagnetic alloy. We compare a system in which the two magnetic constitu-

ents are in contact and consequently antiferromagnetically exchange coupled, and a second system where the two layers are separated by a thick Pt layer to avoid a direct exchange interaction. Our measurements show that the TbFe magnetization reversal strongly depends on the direct interfacial exchange coupling strength and can be dominated either by coherent magnetization reversal processes or by lateral domain formation resulting in domain replication via dipolar interactions.

II. EXPERIMENT PROCEDURES

The two structures studied are [Pt(0.75 nm)/Co(0.25 nm)]₅₀/Tb₃₀Fe₇₀ (25 nm)/Pt(5 nm), referred to below as *A*, where the Co/Pt and TbFe are in contact and a reference [Pt(0.75 nm)/Co(0.25 nm)]₅₀/Pt(3 nm)/Tb₃₀Fe₇₀ (25 nm)/Pt(5 nm), referred to as *B*, where the two magnetic layers are separated by a Pt layer. The samples were deposited by (co)evaporation of the pure metals onto thin 100 nm Si₃N₄ membranes to allow for sufficient penetration of soft x rays in the transmission scattering and microscopy measurements. The [Pt(0.75 nm)/Co(0.25 nm)]₅₀ multilayer exhibits a strong out-of-plane anisotropy, as observed in similar systems.¹⁶ Tb₃₀Fe₇₀ is a ferrimagnetic alloy where the Tb moments are oriented antiparallel to the Fe moments. The system shows a strong perpendicular anisotropy. Its Curie temperature is above room temperature and its net magnetization is dominated by the Tb moments.¹⁷ These three features have been verified by magnetometry measurements on a single Tb₃₀Fe₇₀ alloy film. For instance, the single TbFe layer showed square hysteresis loop as the field was applied perpendicular to the film plane.

In sample *A*, the interfacial exchange interaction between the Pt/Co and TbFe films is dominated by the ferromagnetic Co-Fe exchange interaction, i.e., Co and Fe moments are parallel. As the Tb sublattice moments dominate the total

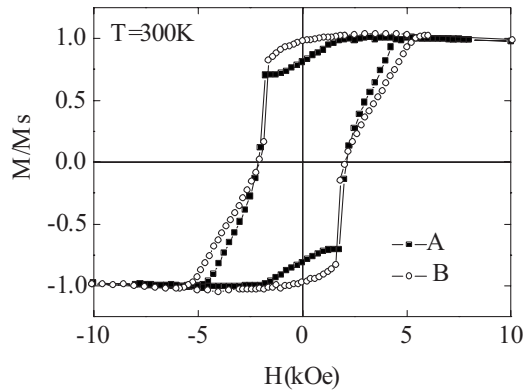


FIG. 1. Hysteresis loops obtained at 300 K with the field perpendicular to the sample surface on samples A, $[\text{Pt}(0.75 \text{ nm})/\text{Co}(0.25 \text{ nm})]_{50}/\text{Tb}_{30}\text{Fe}_{70}$ (25 nm)/Pt(5 nm), (full square) and sample B, $[\text{Pt}(0.75 \text{ nm})/\text{Co}(0.25 \text{ nm})]_{50}/\text{Pt}(3 \text{ nm})/\text{Tb}_{30}\text{Fe}_{70}$ (25 nm)/Pt(5 nm) (Open circle).

$\text{Tb}_{30}\text{Fe}_{70}$ magnetization (i.e., the TbFe average magnetization lays parallel to the Tb moments), the interfacial exchange coupling leads to an antiparallel alignment of the TbFe layer and Pt/Co stack magnetization in the absence of an external field. Introducing a 3 nm Pt layer between the two magnetic materials in sample B effectively suppresses the exchange interaction, and only the dipolar interaction persists between the TbFe layer and Pt/Co stacks. All measurements presented in this paper were performed at room temperature with a field applied perpendicular to the sample surface.

The total magnetization of the samples was measured by superconducting quantum interference device (SQUID) magnetometry. To independently probe the Pt/Co and the TbFe magnetization reversal, various analytical tools based on x-ray magnetic circular dichroism (XMCD) were used at the advanced light source (ALS). The XMCD is a consequence of the different photon absorption cross sections for different orientations between left and right circularly polarized light relative to the sample's magnetization along the photon propagation direction. We utilize the Co and Fe L_3 edges to discriminate between the Pt/Co and TbFe sublayer magnetizations, respectively, noting that the Fe moments are antiparallel to the Tb moments. In the transmission geometry used, signals are proportional to the projection of the magnetization onto the photon propagation direction. Transmission XMCD measurements provide laterally averaged information regarding the magnetization in the constituent sublayers while lateral spatial resolution is obtained by resonant magnetic small-angle scattering from full-field imaging of domains in reciprocal and real spaces, respectively. Further details regarding each technique are given below.

III. EXPERIMENT RESULTS

Figure 1 shows the magnetic hysteresis loops for samples A and B, both normalized to the magnetization M_S obtained for $H=10$ kOe. These measurements provide information about the average magnetization of the samples. The remnant magnetization is nearly equal to the saturation value in the

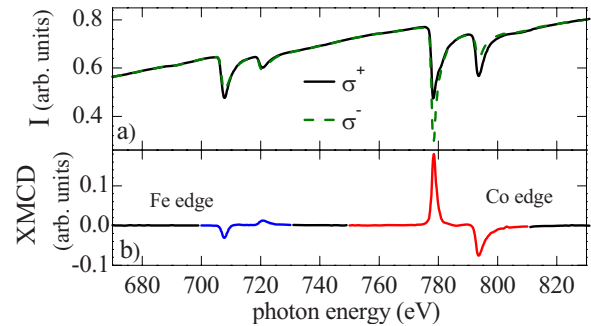


FIG. 2. (Color online) Room-temperature measurements on $[\text{Pt}(0.75 \text{ nm})/\text{Co}(0.25 \text{ nm})]_{50}/\text{Tb}_{30}\text{Fe}_{70}$ (25 nm)/Pt(5 nm) (sample A) in a field of 7 kOe was applied perpendicular to the sample plane: (a) x-ray absorption intensity spectra for both circular polarizations σ^+ and σ^- around 700–800 eV photon energy. (b) XMCD recorded in transmission geometry. The energy spectrum covers the Fe and Co $L_{2,3}$ absorption edges.

case of sample B whereas it is reduced for sample A. This is consistent with an antiferromagnetic alignment of the Pt/Co stack and TbFe layer magnetizations because of the interface exchange coupling in sample A and a parallel alignment for sample B. The evolution of the magnetic configuration is only subtly reflected in differences in the magnetization loops between the two samples.

Figure 2 shows an x-ray absorption and XMCD spectra recorded in transmission geometry for sample A in an applied field of 7 kOe. The energy spectrum covers the Fe and Co $L_{3,2}$ absorption edges between 700–800 eV photon energy. A strong XMCD signal is observed, and its sign reveals an antiparallel alignment between the Co and the Fe moments, which is expected for a parallel alignment of the Pt/Co stack and TbFe layer magnetization at 7 kOe.

Element-selective hysteresis loops shown in Fig. 3 were obtained by measuring the XMCD signal as a function of field at fixed energy either at the Co or Fe L_3 absorption edge at ALS beamline 4.0.2. In Fig. 3 we plot the inverse of the Fe signal where represents the net magnetization of the TbFe layer that is dominated by the Tb moment. The hysteresis loops obtained at the Co edge are alike for both samples, which show that the Pt/Co magnetization is not strongly affected by the interface exchange coupling and the TbFe magnetization reversal. However, the TbFe magnetization reversal is very different for the two samples. For sample B the magnetization loops obtained at the Fe and Co edges are similar, indicating a common reversal mode for the TbFe and Pt/Co layers. Starting from large positive field and decreasing the field, the magnetization stays constant for both layers, and is saturated along the positive field direction until reversal commences at $H=H_{R-B}^{\text{Pt/Co}}$ and $H=H_{R-B}^{\text{TbFe}}$, for which the Pt/Co and TbFe magnetization, respectively, starts to reverse. The reversal of the TbFe layer magnetization takes place at lower field than for the Pt/Co ($H_{R-B}^{\text{TbFe}} < H_{R-B}^{\text{Pt/Co}}$). The slow magnetization decrease for both layers that follows the more abrupt initial reversal (at $H=H_{R-B}^{\text{Pt/Co}}$ and $H=H_{R-B}^{\text{TbFe}}$) are similar to previous observations in perpendicularly magnetized samples¹⁶ and is indicative of the formation of lateral domains created to minimize the dipolar interactions.

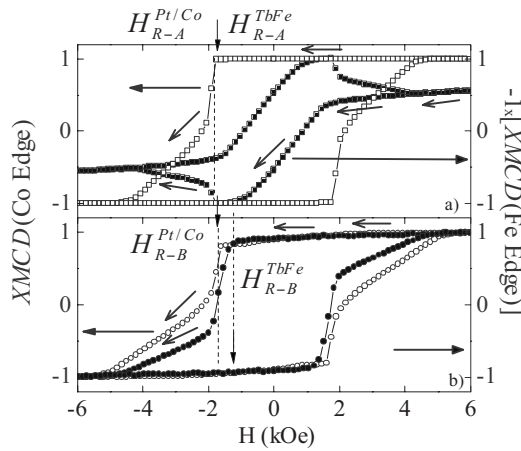


FIG. 3. Normalized XMCD signals at the Co (open red symbols) and Fe (full blue symbols) $L_{2,3}$ edges collected as a function of the field applied perpendicular to the sample plane, and swept from 7 kOe to -7 kOe back to 7 kOe. (a) For $[\text{Pt}(0.75 \text{ nm})/\text{Co}(0.25 \text{ nm})]_{50}/\text{Tb}_{30}\text{Fe}_{70}$ (25 nm)/Pt(5 nm) (sample A) and (b) for $[\text{Pt}(0.75 \text{ nm})/\text{Co}(0.25 \text{ nm})]_{50}/\text{Pt}(3 \text{ nm})/\text{Tb}_{30}\text{Fe}_{70}$ (25 nm)/Pt(5 nm) (sample B), we plot the negative of the Fe signal that reflects the net magnetization of the TbFe layer.

For sample A the magnetization loops obtained at the Fe and Co edges are qualitatively different. Measurements at the Co edge are similar to what was observed for sample B. As the field is swept from large positive field to negative field, the Pt/Co stack magnetization stays constant and saturated until $H_{R-A}^{\text{Pt/Co}}$, where the Co/Pt layer again reserves via domain formation. In contrast, in the field regime where the Co/Pt magnetization is constant, the TbFe layer magnetization continuously decreases with decreasing field (i.e., the XMCD signal at the Fe edge increases). This variation can be characterized by two linear regions with distinct slopes. A small decreasing slope is observed for high fields and a much larger slope for low fields. The decline of the magnetization ends as the negative magnetic saturation is reached for $H > H_{R-A}^{\text{TbFe}}$. At $H = H_{R-A}^{\text{TbFe}}$, which happens to be equal to $H_{R-A}^{\text{Pt/Co}}$ (the reversal field for the Pt/Co), a small part of the TbFe layer magnetization reverses abruptly. This is followed by a small continuous increase of the TbFe magnetization until the Pt/Co stack magnetization saturates. Finally after the saturation of the Pt/Co the TbFe magnetization decreases again and reaches negative saturation.

Although the element specific XMCD measurements depicted in Fig. 3 highlight differences in magnetic behavior of the two samples, they do not give a laterally resolved picture of the magnetization processes. To reach a better understanding of the reversal mechanisms and the cooperative magnetic behaviors operating in both samples, resonant soft x-ray small-angle scattering (SAS) was performed in transmission geometry at ALS beamline 8.0. This is a powerful technique to resolve the lateral magnetic domain structure of magnetic films with perpendicular anisotropy, with chemical selectivity allowed by tuning the photon energy to the x-ray absorption edges.^{7,9,18} We utilized linearly (s) polarized incident radiation, whose scattered intensity contains contributions from magnetic-magnetic and charge-charge correlations

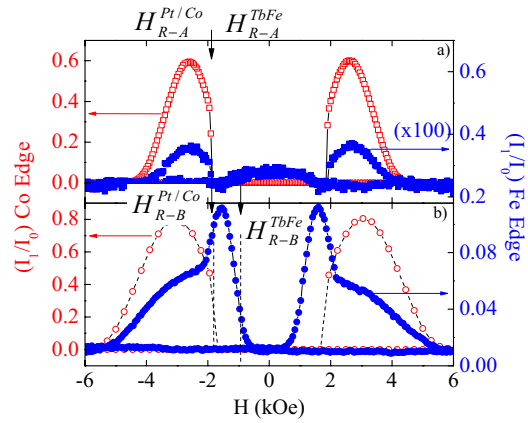


FIG. 4. (Color online) Normalized soft x-ray small-angle scattering intensity observed at the Co $L_{2,3}$ (open red symbols) and at the Fe $L_{2,3}$ edges (full blue symbols) as a function of the field applied perpendicular to the sample plane and swept from 7 kOe to -7 kOe back to 7 kOe (a) for $[\text{Pt}(0.75 \text{ nm})/\text{Co}(0.25 \text{ nm})]_{50}/\text{Tb}_{30}\text{Fe}_{70}$ (25 nm)/Pt(5 nm) (sample A) and (b) for $[\text{Pt}(0.75 \text{ nm})/\text{Co}(0.25 \text{ nm})]_{50}/\text{Pt}(3 \text{ nm})/\text{Tb}_{30}\text{Fe}_{70}$ (25 nm)/Pt(5 nm) (sample B).

but not magnetic-charge cross correlations.¹⁹ Symmetric transmission geometry scattering constrained the direction of the scattering vector \mathbf{q} in the film plane and its value (0.03 nm^{-1}) to approximately 2π over the domain periodicity in Pt/Co multilayers to optimize coupling to the lateral domain structure.¹⁸ SAS intensity was measured as a function of the magnetic field applied perpendicular to the film plane (Fig. 4). For a uniformly magnetized film, there will be no magnetic SAS intensity, and when tuned to the Co edge, the intensity drops to zero when the sample is saturated. At the Fe edge, small but finite intensity is observed when the sample is nominally saturated; this results from residual charge-charge scattering independent of magnetism. In this geometry, the SAS intensity for a given \mathbf{q} increases as that spatial frequency component of lateral domains increases.¹⁸ The photon energy was tuned to collect data at the maximum in the Co and Fe L_3 absorption edges.

As for the XMCD measurements, the SAS intensities at the Co edge are quite similar for samples A and B (Fig. 4). After saturation in positive field, the scattering intensity starts to increase at a field close to $H_{R-A}^{\text{Pt/Co}} \approx H_{R-B}^{\text{Pt/Co}}$, reaches a maximum around 3.5 kOe, and falls back to its minimum at a saturation field consistent with that determined by SQUID and XMCD measurements. These measurements agree with previous studies of Pt/Co multilayer magnetization reversal by labyrinthine stripe domain formation for $H = H_{R-A}^{\text{Pt/Co}}$ or $H_{R-B}^{\text{Pt/Co}}$, followed by domain annihilation with the domain period constant throughout.^{7,9,18}

Scattering measurements at the Fe edge are again quite different between the two samples. From positive to negative saturation, scattering from sample B first appears at $H = H_{R-B}^{\text{TbFe}}$ while the Pt/Co is still saturated and increases to a maximum for $H_{R-B}^{\text{TbFe}} > H > H_{R-B}^{\text{Pt/Co}}$. This initial domain formation in TbFe is independent from that in Pt/Co. However, it is clearly seen that the evolution of the TbFe domains is strongly perturbed when domains form in the Pt/Co stack at

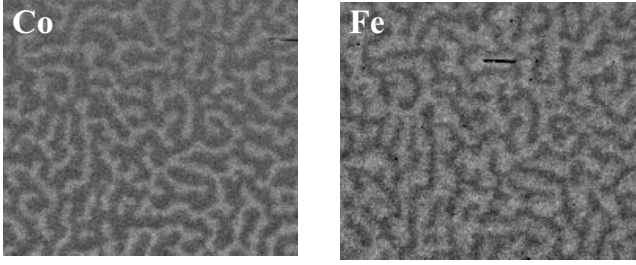


FIG. 5. Magnetic x-ray microscopy images (field of view about $6 \mu\text{m}$) recorded at the Co L_3 (left) and Fe L_3 edges (right) at an external magnetic field $H = -3$ kOe. The two images show the same domain pattern with reversed contrast demonstrating the antiparallel alignment of the Fe and Co moments.

$H = H_{R-B}^{\text{Pt/Co}}$. The Co and Fe signals saturate at similar fields. For sample A, the signal obtained at the Fe edge is 300 times weaker than that at the Co edge, suggesting that the domains formed in the TbFe layers are either not fully magnetized normal to the film or small in number. Nevertheless the shape of the signal at the Co and Fe edge are qualitatively similar.

The close correlation between the SAS intensities observed in sample B suggests a correlated domain structure presumably driven by the dipolar interactions. To verify the influence of the dipolar interaction on the magnetic configuration during field cycles, high-resolution magnetic soft x-ray transmission microscopy (MXTM) was used to image layer resolved details of the magnetic domain structure in the Pt/Co multilayer and TbFe layers. The experiments were carried out at XM-1 at ALS beamline 6.1.2.²⁰ Fresnel zone plates used as x-ray optical elements have demonstrated a spatial resolution down to 15 nm.^{21,22} For this experiment the x-ray optics had a spatial resolution of 30 nm. Magnetic contrast is again provided by the XMCD effect occurring at the respective Fe (706 eV) and Co (777 eV) L_3 edges.

Figure 5 displays two x-ray images covering a field of view of about $6 \mu\text{m}$, and recorded at the same sample position for the Co L_3 [Fig. 5(a)] and Fe L_3 edges [Fig. 5(b)], thereby displaying the Fe and the Co magnetic domain structures separately in each magnetic layer. The images were recorded at an external magnetic field $H = -3$ kOe field, i.e., at a field where domains are formed in both TbFe and Pt/Co layers. Since the contrast is given by the projection of the magnetization along the photon propagation direction, here, perpendicular to film plane, the dark and light areas correspond to the “up” and “down” directions of the domain magnetization (relative to the sample’s surface). Both MXTM images show a labyrinthine magnetic domain structure with domain size of about 200 nm. Remarkably, the down domains at the iron edge match exactly, in position and shape, with the up domains at the Co edge and vice versa. This is a direct proof that the Co moments of the Pt/Co stack and the Fe moments of the TbFe layer are aligned antiparallel to each other. This is also in agreement with the expectation that the stray field triggers the stripe domain formation in both uncoupled layers, and is strong enough to couple them via dipolar interaction through the thick Pt interlayer.^{23–25} These layer resolved high-resolution magnetic soft x-ray micros-

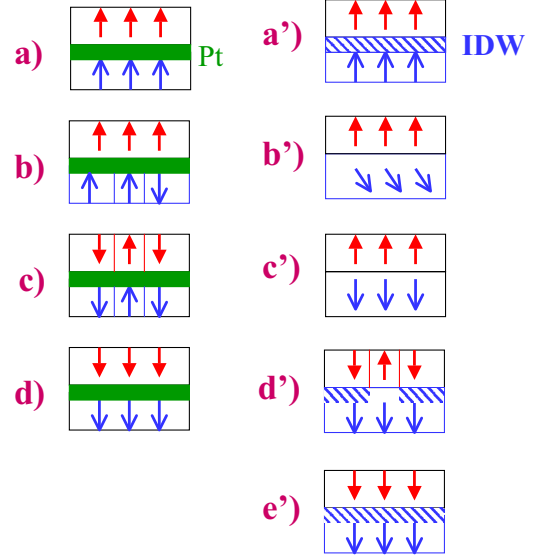


FIG. 6. (Color online) Schematic magnetic configurations starting from large positive saturation. For $[\text{Pt}(0.75 \text{ nm})/\text{Co}(0.25 \text{ nm})]_{50}/\text{Pt}(3 \text{ nm})/\text{Tb}_{30}\text{Fe}_{70}$ (25 nm)/Pt(5 nm) (sample B), we have: (a) $H > H_{R-B}^{\text{TbFe}}$: the Pt/Co and the TbFe magnetizations are parallel and saturated out of plane along the positive field direction. (b) $H_{R-B}^{\text{TbFe}} > H > H_{R-B}^{\text{Pt/Co}}$: the Pt/Co magnetization is saturated. Lateral domains form in the TbFe layer. (c) $H < H_{R-B}^{\text{Pt/Co}}$: lateral domains form in the Pt/Co magnetization and replicate domains in the TbFe. (d) $H > 6$ kOe: both the Pt/Co and TbFe magnetizations saturate along the negative field direction. For $[\text{Pt}(0.75 \text{ nm})/\text{Co}(0.25 \text{ nm})]_{50}/\text{Tb}_{30}\text{Fe}_{70}$ (25 nm)/Pt(5 nm) (sample A), we have: (a') $H > 1.5$ kOe: the Pt/Co and the TbFe magnetizations tend to be parallel along the positive field direction applied perpendicular to the sample plane; consequently an IDW is present at the interface in the TbFe. (b') 1.5 kOe $< H < 1.5$ kOe: TbFe layer magnetization coherently rotates while the Pt/Co stack is still saturated. (c') $H = H_{R-A}^{\text{TbFe}} = H_{R-A}^{\text{Pt/Co}}$: the two magnetizations are saturated and antiparallel. (d') $H < H_{R-A}^{\text{Pt/Co}}$: domains form in the Pt/Co layer; consequently lateral regions with and without an IDW coexist in the TbFe layer. (e') $H < 5$ kOe: the Pt/Co and the TbFe magnetizations tend to be parallel along the negative field direction applied perpendicular to the sample plane; consequently, an IDW is present at the interface in the TbFe.

copy images constitute direct imaging of dipolar field induced domain replication in perpendicularly magnetized system. Images obtained at an external magnetic field of 1.5 kOe confirmed the presence of domains in the TbFe and no domains in the Pt/Co multilayer in agreement with the scattering results.

IV. DISCUSSION

These complementary measurements permit us to determine the following reversal modes. For sample B the reversal mode is straight forward. For $H > H_{R-B}^{\text{TbFe}}$ the Pt/Co and the TbFe magnetizations are parallel and saturated out of plane [Fig. 6(a)]. For $H_{R-B}^{\text{TbFe}} > H > H_{R-B}^{\text{Pt/Co}}$, the Pt/Co magnetization is still saturated; however the TbFe magnetization decreases and the SAS intensity evidences the formation of lateral domains in the TbFe layer [Fig. 6(b)]. This indicates that the

TbFe layer is reversing via nucleation and domain propagation, as expected for perpendicular anisotropy films. Because $\text{Tb}_{30}\text{Fe}_{70}$ at room temperature has a small net magnetization,¹⁷ the stray field it is generating is not strong enough to nucleate domains in the Pt/Co stack. For $H < H_{R-B}^{\text{Pt/Co}}$, domains nucleate in the Pt/Co and the magnetization decreases. As the Pt/Co domains appear they create strong dipolar fields that perturb the TbFe domains, leading to domain replication [Fig. 6(c)]. Finally at similar applied field, both the Pt/Co and TbFe magnetizations saturate [Fig. 6(d)].

For sample A the reversal mode is not as obvious. Before $H = H_{R-A}^{\text{TbFe}} = H_{R-A}^{\text{Pt/Co}}$ is reached, the measurements suggest that no lateral domains are formed in either layer and that the Pt/Co magnetization is saturated; however the TbFe magnetization decreases in positive field. To explain this behavior one has to consider that to minimize the exchange interaction and the Zeeman energy, an interface domain wall (IDW) has to be created.^{26,27} This IDW is laterally uniform and mainly located in the TbFe layer [Fig. 6(a)]. This implies that the energy of an IDW in the TbFe is smaller than in Pt/Co, which is expected since at room temperature the magnetization, anisotropy, and exchange stiffness is lower for the TbFe alloy than for the Pt/Co multilayer.

Under large positive fields the IDW thickness is small and is compressed against the Co/Pt. As the applied field decreases the IDW thickness increases as it “decompresses.” Such IDW has been recently observed in similar perpendicular magnetized sample using polarized neutron reflectometry.²⁸ This effect explains the gradual decrease in the TbFe magnetization. The change in the magnetization slope may be explained by a change in the TbFe magnetization reversal: from IDW decompression to coherent rotation [Fig. 6(b)] as the domain wall approaches the TbFe film thickness. Then for fields close to $H = H_{R-A}^{\text{TbFe}} = H_{R-A}^{\text{Pt/Co}}$, the two magnetizations are saturated and antiparallel [Fig. 6(c)]; at this stage the IDW is no longer present and the exchange energy is minimized as expected in zero applied field. For $H < H_{R-A}^{\text{Pt/Co}}$, domains form in the Pt/Co layer, which give rise to an SAS intensity. As domains form in the Pt/Co, it is to be expected that domains should also nucleate in the TbFe.

While there is evidence for this in the scattering results (Fig. 4), the intensity is extremely low, suggesting a small fraction of the TbFe layer is forming domains. This was understood by the formation of lateral regions with and without an IDW present [Fig. 6(d)]. Most of the TbFe layers maintain a uniform magnetization and the frustrated exchange coupling results in local domain walls. Such a magnetic configuration was predicted for imperfect ferromagnetic/antiferromagnetic interfaces.²⁹ The presence of those interfacial domain walls explain why the XMCD signal at the Fe edge decreases for $H < H_{R-A}^{\text{Pt/Co}}$ while domain reversal is observed in the Pt/Co layer. Finally for $H < 5$ kOe, the Pt/Co and the TbFe magnetizations tend toward the negative field direction. As the field increases, the Zeeman energy increases relatively to the interfacial exchange coupling energy, leading to the compression of the IDW. Figure 3(a) clearly indicates that the domain wall is only contained in the TbFe [as shown on Fig. 6(d)] since the XMCD signal at the Co edge is maximum while the XMCD signal at the Fe edge increases slowly toward saturation.

In conclusion, we have performed a study on the influence of a direct antiferromagnetic exchange coupling in perpendicularly magnetized model systems. The use of complementary advanced synchrotron-radiation techniques allowed us to probe each magnetic layer independently and to obtain element specific domain images. In a reference uncoupled bilayer the formation of lateral domains was observed. The domains inside the Pt/Co multilayer were found to produce a stray field sufficient to induce lateral domain in the TbFe layer. Direct evidence of this replication effect was obtained. In exchange-coupled bilayers, the magnetization reversal process is dramatically different. These experimental results could be understood assuming that an interface domain wall is created, and that the TbFe magnetization reversal is then dominated by domain-wall compression and coherent magnetization reversal processes.

ACKNOWLEDGMENTS

We thank O. Hellwig for helpful discussions. This work was supported by the Director, Office of Science, Office of Basic Energy Sciences of the U.S. Department of Energy under Contracts No. DE-AC02-05-CH11231.

¹J. Nogues and I. K. Schuller, *J. Magn. Magn. Mater.* **192**, 203 (1999).

²Eric E. Fullerton, J. S. Jiang, C. H. Sowers, J. E. Pearson, and S. D. Bader, *Appl. Phys. Lett.* **72**, 380 (1998).

³T. Hauet, J. A. Borchers, Ph. Mangin, Y. Henry, and S. Mangin, *Phys. Rev. Lett.* **96**, 067207 (2006).

⁴J. C. Kools, *IEEE Trans. Magn.* **32**, 3165 (1996).

⁵J.-U. Thiele, S. Maat, and E. E. Fullerton, *Appl. Phys. Lett.* **82**, 2859 (2003).

⁶O. Hellwig, A. Berger, and E. E. Fullerton, *Phys. Rev. Lett.* **91**, 197203 (2003).

⁷O. Hellwig, A. Berger, J. B. Kortright, and E. E. Fullerton, *J. Magn. Magn. Mater.* **319**, 13 (2007).

⁸C. Kittel, *Phys. Rev.* **70**, 965 (1946); *Rev. Mod. Phys.* **21**, 541 (1949).

⁹O. Hellwig, T. L. Kirk, J. B. Kortright, A. Berger, and E. E. Fullerton, *Nat. Mater.* **2**, 112 (2003).

¹⁰K. Janicka, J. D. Burton, and E. Y. Tsymbal, *J. Appl. Phys.* **101**, 113921 (2007).

¹¹A. Baruth, L. Yuan, J. D. Burton, K. Janicka, E. Y. Tsymbal, S. H. Liou, and S. Adenwalla, *Appl. Phys. Lett.* **89**, 202505 (2006).

¹²Meng-Shian Lin and Chih-Huang Lai, *J. Appl. Phys.* **101**, 09D121 (2007).

¹³U. K. Rossler and A. N. Bogdanov, *J. Appl. Phys.* **101**, 09D105 (2007).

- ¹⁴A. N. Bogdanov, A. V. Zhuravlev, and U. K. Rossler, *Phys. Rev. B* **75**, 094425 (2007).
- ¹⁵N. S. Kiselev, I. E. Dragunov, U. K. Roessler, and A. N. Bogdanov, *Appl. Phys. Lett.* **91**, 132507 (2007).
- ¹⁶D. Weller, L. Folks, M. Best, Eric. E. Fullerton, B. D. Terris, and G. J. Kusinski, *J. Appl. Phys.* **89** 7525 (2001).
- ¹⁷P. Hansen, C. Clausen, G. Much, M. Rosenkranz, and K. Witter, *J. Appl. Phys.* **66**, 756 (1989).
- ¹⁸J. B. Kortright, Sang-koog Kim, G. P. Denbeaux, G. Zeltzer, K. Takano, and Eric E. Fullerton, *Phys. Rev. B* **64**, 092401 (2001).
- ¹⁹J. B. Kortright, O. Hellwig, K. Chesnel, S. Sun, and E. E. Fullerton, *Phys. Rev. B* **71**, 012402 (2005).
- ²⁰P. Fischer, D. H. Kim, B. L. Mesler, W. Chao, and E. H. Anderson, *J. Magn. Magn. Mater.* **310**, 2689 (2007).
- ²¹D.-H. Kim, P. Fischer, W. Chao, E. Anderson, M.-Y. Im, S.-C. Shin, and S.-B. Choe, *J. Appl. Phys.* **99**, 08H303 (2006).
- ²²W. Chao, B. H. Harteneck, J. A. Liddle, E. H. Anderson, and D. T. Attwood, *Nature (London)* **435**, 1210 (2005).
- ²³V. Baltz, A. Marty, B. Rodmacq, and B. Dieny, *Phys. Rev. B* **75**, 014406 (2007).
- ²⁴M. Hehn, O. Lenoble, D. Lacour, and A. Schuhl, *Phys. Rev. B* **62**, 11344 (2000).
- ²⁵T. Hauet, C. M. Günther, B. Pfau, M. E. Schabes, J.-U. Thiele, R. L. Rick, P. Fischer, S. Eisebitt, and O. Hellwig, *Phys. Rev. B* **77**, 184421 (2008).
- ²⁶F. Montaigne, S. Mangin, and Y. Henry, *Phys. Rev. B* **67**, 144412 (2003).
- ²⁷S. Mangin, C. Bellouard, S. Andrieu, F. Montaigne, P. Ohresser, N. B. Brookes, and B. Barbara, *Phys. Rev. B* **70**, 014401 (2004).
- ²⁸S. M. Watson, T. Hauet, J. A. Borchers, S. Mangin, and Eric E. Fullerton, *Appl. Phys. Lett.* **92**, 202507 (2008).
- ²⁹A. Berger and E. E. Fullerton, *J. Magn. Magn. Mater.* **165**, 471 (1997).